Accurate Local Blood Flow Measurements with Dynamic PET: Fast Determination of Input Function Delay and Dispersion by Multilinear Minimization

J. van den Hoff, W. Burchert, W. Müller-Schauenburg, G.-J. Meyer and H. Hundeshagen

Abteilung Nuklearmedizin und spezielle Biophysik, Zentrum Radiologie, Medizinische Hochschule Hannover, Hannover, Germany and Abteilung Nuklearmedizin der Radiologischen Klinik, Universität Tübingen, Tübingen, Germany

Accurate determination of local blood flow in tissue using the Kety-Schmidt one-compartment model for freely diffusible tracers requires knowledge of the true arterial input function in tissue. Because measured input functions are usually delayed and dispersed with respect to true influx, a correction of the experimental input function is necessary. We describe a technique that uses a fast multilinear least-squares minimization procedure to determine simultaneously the dispersion, the blood flow and the partition coefficient as a function of delay. In this approach, a few multilinear fits are sufficient to determine the complete set of parameters necessary to describe the data. Because of the high speed of the procedure, dispersion effects may be taken into account on a pixel-by-pixel basis in calculating parametric images of blood flow and partition coefficient. The described procedure has been used at our institute for about 1 yr in more than 160 investigations and has proven well suited for routine use in a clinical environment.

J Nucl Med 1993; 34:1770–1777

Dynamic positron emission tomography (PET) offers a unique noninvasive method for reliable quantitative determination of local blood flow in tissue using tracers such as ^{15}O-labeled water or butanol which can be considered as nearly free diffusible under physiological conditions (*16,17*).

In addition to the time-activity curve in tissue derived from the dynamic PET scan (tissue-response function), the time-activity curve in arterial blood (arterial-input function) must also be known. In most cases this information can only be derived from arterial blood sampling at a peripheral site such as the radial artery. To enable unbiased estimations of the interesting physiological parameters, i.e., blood flow and tissue-blood partition coefficient, one must derive the true input function in tissue from the measured input function. Two related effects have to be considered in this context (*1–6,13–15*), namely delay and dispersion.

Delay is caused by the differing path lengths the tracer has to travel from the heart to either sampling site or target organ. The measured input function is therefore shifted (usually delayed) with respect to the true input function. Moreover, the tracer bolus experiences a smearing out (dispersion) due to inhomogeneous velocity fields in the vessels which differs for measured and true input function.

Several approaches have been proposed to correct these effects. These approaches suffer from different drawbacks in either validity or computing-time efficiency (*1–6*).

This study describes a numerically, stable and fast procedure that allows a consistent simultaneous determination of all parameters in the model and enables simultaneous calculation of parametric images of blood flow and partition coefficient.

MATERIALS AND METHODS

Data Acquisition

The PET data were acquired with a *Siemens ECAT 951/31 PET* scanner. Thirty-one slices with a plane separation of 3.4 mm were obtained simultaneously. The axial and transaxial resolution of the reconstructed image (Hann-filter, cut-off frequency 0.4, 128 × 128 matrix) was about 7–8 mm FWHM.

After a bolus injection of 3.7 GBq ^{15}O-H_2O, multiple time frames were taken (12 × 5 sec, 4 × 30 sec). The total scan time was 3 min. The method for synthesis and the automated procedure for the application of the ^{15}O-labeled water has been described before (*18*). All image data were corrected for attenuation (10 min transmission) and decay during the reconstruction procedure.

Radial artery blood samples (1 ml) were taken according to the dynamic protocol at midframe times and one immediately before start of the scan. The samples were counted in a wellcounter which was cross-calibrated to the PET scanner. The decay-corrected values were transferred to a SUN 4-workstation for further data processing.

Received Nov. 6, 1992; revision accepted June 17, 1993.

For correspondence and reprints contact: J. van den Hoff, PhD, Abteilung Nuklearmedizin und spezielle Biophysik, Zentrum Radiologie, Medizinische Hochschule Hannover, Konstanty-Gutschow-Str. 8, 3000 Hannover 61, Germany.

Theory

The kinetics of a freely diffusible tracer is governed by the linear differential equation of the Kety-Schmidt model (*11*). The relation between the true arterial input function $c_a(t)$ and the tissue response function $c_i(t)$ is given by:

$$\dot{c}_i(t) = fc_a(t) - \frac{f}{p} c_i(t), \qquad \text{Eq. 1}$$

where f is blood flow, p is tissue blood partition coefficient and the time derivative is indicated by a dot. (Decay-corrected quantities are considered throughout.) The analytic solution of Equation 1 is:

$$c_i(t) = fc_a(t) * e^{-kt} = fe^{-kt} \int_0^t c_a(s)e^{ks}\, ds, \qquad \text{Eq. 2}$$

where $k = f/p$ and * denotes convolution. This equation depends nonlinearily on k, which necessitates the use of time-consuming iterative minimization procedures (usually of the Levenberg-Marquardt type (*7*)) in order to derive estimates for f and k directly from Equation 2.

If on the other hand an integration of Equation 1 is performed, observing that $c_i(0) = 0$), the equivalent integral equation:

$$c_i(t) = f \int_0^t c_a(s)\, ds - k \int_0^t c_i(s)\, ds, \qquad \text{Eq. 3}$$

is obtained. Equation 3 offers the opportunity to determine f and k (hence p) from a linear two-parameter fit by treating the time-dependent integrals as known basis functions in a fit to the model function:

$$c_i(t) = fj_a(t) - kj_i(t), \qquad \text{Eq. 4}$$

where:

$$j_a(t) = \int_0^t c_a(s)\, ds \text{ and } j_i(t) = \int_0^t c_i(s)\, ds.$$

This possibility was first recognized by Blomqvist (*8*).

The Influence of Delay and Dispersion

As already noted by Meyer (*3*), consecutive corrections for delay and dispersion in general will not be selfconsistent, i.e., reversal of the order of corrections will yield different results. Such procedures can only determine the correct values if the dependence of the goodness-of-fit parameter χ^2 (the sum of the squared differences between data and fit) on delay and dispersion is such that the absolute minimum of χ^2 can be determined by two independent one-dimensional minimizations. Because in general this is not the case, a consistent approach is called for in which the correct relation between experimental and true input function is taken into account.

It should be noted that only the dispersion of the measured input function $c_m(t)$ relative to the true $c_a(t)$ in tissue is of interest, not the total dispersion of the injected bolus prior to the sampling. This implies that under reasonable experimental conditions, dispersion is a minor effect compared to delay, and the shape of $c_m(t)$ will always be similar to that of $c_a(t)$. Therefore, it is justified to describe dispersion according to Iida et al. (*4*) by the convolution:

$$c_m(t) = c_a(t) * \frac{e^{-t/\tau}}{\tau}, \qquad \text{Eq. 5}$$

so that the effect of dispersion is completely specified by the dispersion time constant τ. A direct consequence of Equation 5 is:

$$c_a(t) = c_m(t) + \tau \dot{c}_m(t), \qquad \text{Eq. 6}$$

as can be seen by performing the convolution in Equation 5 and computing the time derivative.

Delay is taken into account by shifting the time scale of $c_m(t)$ in Equation 6 by the delay time Δ (by convention Δ is positive if $c_m(t)$ is delayed with respect to $c_a(t)$):

$$c_a(t) = c_m(t + \Delta) + \tau \dot{c}_m(t + \Delta). \qquad \text{Eq. 7}$$

This is the required relation between measured and true input function. The most straightforward way to proceed is to insert Equation 7 in Equation 2 and perform a nonlinear least-squares fit for the set of parameters (f, p, τ, Δ), as described by Meyer (*3*).

The Multilinear Approach

The ultimate goal of investigating regional differences of blood flow is generation of parametric images for blood flow and partition coefficient. Nonlinear fitting is too slow to allow calculation of parametric images even if the parameters τ and Δ are fixed according to results obtained on a representative region. One therefore has to resort to some other procedure, such as weighted integration techniques (*9*) once τ and Δ have been determined by the nonlinear fit.

We investigated whether a unified procedure could be found that enables sufficiently fast fits even on a pixel-by-pixel basis. We found that this can be achieved by combining Equation 7 and Equation 3. This yields (observing that $c_m(\Delta) = 0$):

$$c_i(t) = \varepsilon c_m(t + \Delta) + f \int_0^t c_m(s + \Delta)\, ds - k \int_0^t c_i(s)\, ds$$

$$= \varepsilon c_m(t + \Delta) + fj_m(t, \Delta) - kj_i(t), \text{ with } \varepsilon = f\tau. \qquad \text{Eq. 8}$$

Comparison with Equations 3 and 4 show that dispersion introduces an additional term εc_m in the model equation. Given the experimental determined functions $c_m(t)$ and $c_i(t)$, Equation 8 allows fast simultaneous determination of parameters ε, f and k for any fixed delay Δ by means of a three-parameter linear least-squares fit. One can proceed by performing a series of fits to Equation 8 in which the whole range of possible values for Δ is scanned. The minimum of the function $\chi^2(\Delta, \varepsilon(\Delta), f(\Delta), k(\Delta))$ thus found yields the best estimates for the complete set of parameters.

Graphical Quality Control

We introduced elsewhere (*10*) a linearized representation of data that enables a sensitive check with respect to possible errors in delay and dispersion corrections: dividing both sides of Equation 3 by $[\int_0^t c_a(s)\, ds]$, the equation is transformed to a straight line:

$$y(x) = f - kx, \qquad \text{Eq. 9}$$

where y(t) and x(t) are defined by:

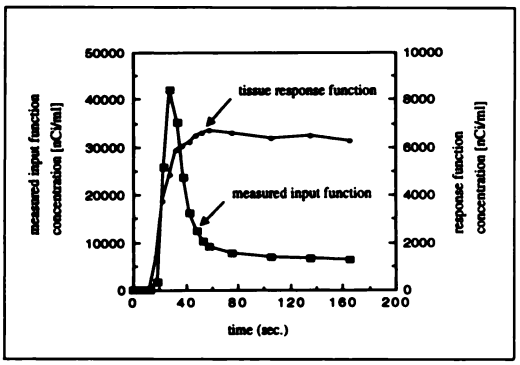

FIGURE 1. Experimental input function and tissue response from a grey matter region of the human brain. Different scales are used for input and response function.

$$y(t) = \frac{c_i(t)}{\int_0^t c_a(s)\,ds} = \frac{c_i(t)}{j_a(t)},\quad x(t) = \frac{\int_0^t c_i(s)\,ds}{\int_0^t c_a(s)\,ds} = \frac{j_i(t)}{j_a(t)}.$$

Eq. 10

In this representation blood flow appears as the y-intercept and the partition coefficient as the x-intercept of the straight line y(x). (This transformation has been introduced independently by Yokoi et al. (*12,19*)).

Using the experimental input function and assuming delay and dispersion according to Equation 7, the definition of x(t) and y(t) can be reformulated to yield:

$$y(t) = \frac{c_i(t)}{j_m(t, \Delta) + \tau \cdot c_m(t + \Delta)},\quad x(t) = \frac{j_i(t)}{j_m(t, \Delta) + \tau \cdot c_m(t + \Delta)},$$

where

$$j_m(t, \Delta) = \int_0^t c_m(s + \Delta)\,ds. \qquad \text{Eq. 11}$$

If one plots experimental data in the form y(x) according to Equation 11 using the values of delay and dispersion as determined by the above described fitting procedure, the data will follow the straight line of Equation 9 only if τ and Δ values are correct.

Computer Simulations

It is understood that temporal sampling both for the arterial input function and tissue response is sufficiently fine so that uncertainties connected with interpolation and numerical integration of the discretely sampled data are insignificant. Then, as is obvious from the derivation of Equation 8, the described procedure is exact as far as noiseless data are concerned. The multilinear approach therefore gives unbiased estimates of the underlying true parameters of the data set.

Presence of statistical noise in the data alters this situation: noise might lead to systematic errors in parameter estimates because in least-squares fitting it is presupposed that the basis functions of the model (c_m, j_m, j_i in Equation 8) are exact. This assumption is fulfilled to a good approximation for $c_m(t)$ and $j_m(t)$. However, $j_i(t)$ exhibits substantial noise if individual pixels are involved, even if one recognizes that the relative uncertainties in $j_i(t)$ are much smaller than those of $c_i(t)$, due to the smoothing effect of the involved integration. We therefore investigated the influence of noisy data on the parameter estimates by means of Monte Carlo simulations. For this purpose we superimposed Gaussian-shaped noise distributions of varying width on theoretical tissue response curves which were generated via Equation 2 for several values of parameters f and k from a typical experimental input function.

RESULTS

Performance of the Multilinear Approach

A typical experimental input function with the tissue response from a grey matter region in brain is shown in Figure 1. Both curves are drawn at a different scale to show the onset of tissue response. Figure 2A shows the tissue-response data and the optimal fit to Equation 8, assuming a fixed value of $\tau = 0$. Figure 2B shows the linearized representation of the data (input plus response) in the form y(x) along with the straight line according to Equation 9 using the fitted values of f and k. The values of blood flow and partition coefficient can be read as axes intercepts. Systematic deviation of the data from the line at small x (corresponding to early times) is obvious and indicates that dispersion has not been adequately considered. In Figure 2A the corresponding deviations at early times are much more difficult to detect.

Using the correct procedure of fitting the complete set of parameters leads to the results presented in Figures 3A and 3B where data points follow the theoretical expected behavior much better. Figure 4 shows the corresponding true input function that results from the explicit deconvolution

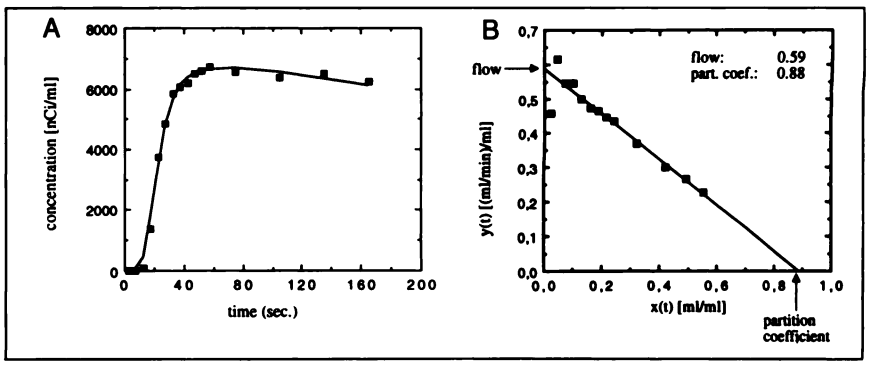

FIGURE 2. (A) Tissue response from Figure 1 together with fit according to Equation 8. Input function delay Δ is optimized in the fit (Δ_{opt} = 8.6 sec), whereas dispersion τ is neglected. (B) Linearized representation of the data from (A) according to Equations 9 and 11. Axes intercepts of the straight line yield flow and partition coefficient.

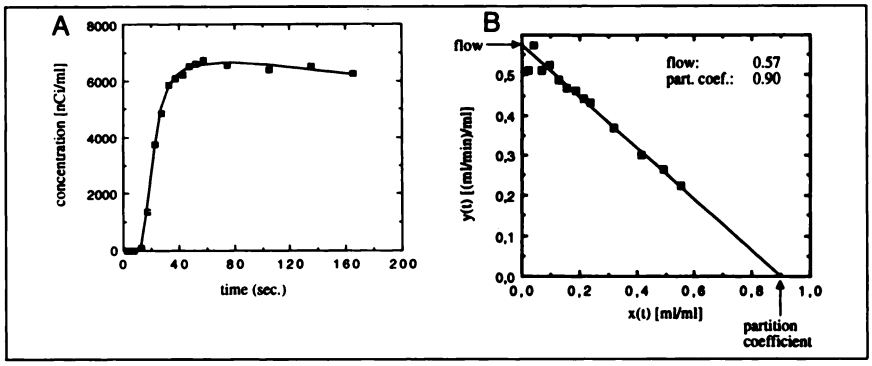

FIGURE 3. (A) Tissue response from Figure 1 together with fit according to Equation 8. Input function delay Δ and dispersion τ are optimized in the fit (Δ_{opt} = 4.8 sec, τ_{opt} = 4.3 sec). (B) Linearized representation of the data from (A) according to Equations 9 and 11. Systematic deviations from the straight line are reduced at small x as compared to Figure 2B.

according to Equation 7 using the derived values of Δ and τ.

The neglect of dispersion (i.e., setting $\tau = \varepsilon = 0$ in the fitting procedures) results in systematic errors for blood flow and partition coefficient which usually amount to only a few percent if the delay is adjusted freely. To demonstrate this more clearly, the function $\chi^2(\Delta)$ is shown in Figure 5A as it results from the series of fits to Equation 8 if $\varepsilon = 0$ is assumed. The minimum of $\chi^2(\Delta)$ corresponds to the best value Δ = 8.6 sec, which leads to results in Figure 2. In Figure 5B the same function is plotted if ε is optimized in the fit. Now there is a relatively large range of Δ-values for which the fit remains quite good. The minimum corresponds to results in Figures 3A and 3B. The blood flow f and the partition coefficient p are rather insensitive to the variation of Δ if ε is optimized to compensate for this variation. This means that a mismatch of one parameter can be compensated to a certain extent by an appropriate change in the other, as can be seen by comparing results in Figures 2B and 3B. However, the most accurate values are obtained if Δ and ε are fitted simultaneously.

Finally, the sensitivity of the linearized representation with regard to a mismatch of Δ is demonstrated in Figures 6A and 6B. Delay has been fixed to a value of 5 sec (as compared to the best value of 8.6 sec) (Fig. 2B). Deviations from the straight line in Figure 6B show that the 'delay correction' is insufficient, whereas the quite small deviations between fit and data in Figure 6A might lead to the conclusion that the fit is acceptable. A comparison with Figure 2 indicates that this would result in systematic errors of about 12% for blood flow and 6% for the partition coefficient.

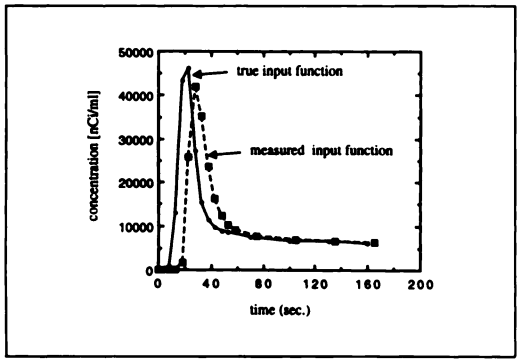

FIGURE 4. Measured input function and true input function which results after correction of delay and dispersion.

Typical parametric images obtained by our approach are shown in Figures 7 and 8. The investigation was performed postoperatively in a patient with stenosis of the left middle cerebral artery. In Figure 7 the blood flow image shows a significantly better resolution and reduced noise level compared to the partition coefficient image in Figure 8. This is explained by the fact that blood flow is directly determined by the fit, whereas the partition coefficient is computed from the ratio of the fit parameters f and k.

The computation of the parametric images (128 × 128 pixels) together with images of parameter standard deviations and the χ^2 takes about 20 sec on a SUN SPARCstation.

Results derived in investigations of patients with stenosis of the middle cerebral artery are shown in Table 1. Reduction of the average flow in the parietal cortex is evident as is reduction in the average partition coefficient.

Results of the Monte Carlo Simulations

Gaussian-shaped noise distributions of varying width were superimposed on theoretical tissue-response curves generated via Equation 2 for several values of blood flow and partition coefficient from a typical experimental input function. The frequency distributions of the fit parameters are directly derived by applying the multilinear approach to a sufficiently large number of simulated noisy data sets. In these simulations we used the following relation between the squared standard deviation (s.d.) of the noise distribution and the count rate (CTR) in an individual pixel or region of interest (ROI) of the reconstructed image:

$$\text{s.d.}^2 = \text{const.} * \text{CTR}.$$

The proportionality constant was adjusted to various values in several runs of simulations. These investigations lead to the conclusion that our approach remains valid even at very high noise levels, as in the case of individual pixels.

Figure 9 shows the simulated noise-free tissue response for a flow of 0.5 (ml/min)/ml and a partition coefficient of 0.9 ml/ml. Also shown is one of the noisy tissue-response curves generated in this simulation. The noise level (s.d./CTR = 20% in the maximum of the noise-free response curve) is typical for per-pixel count rates obtained in LCBF

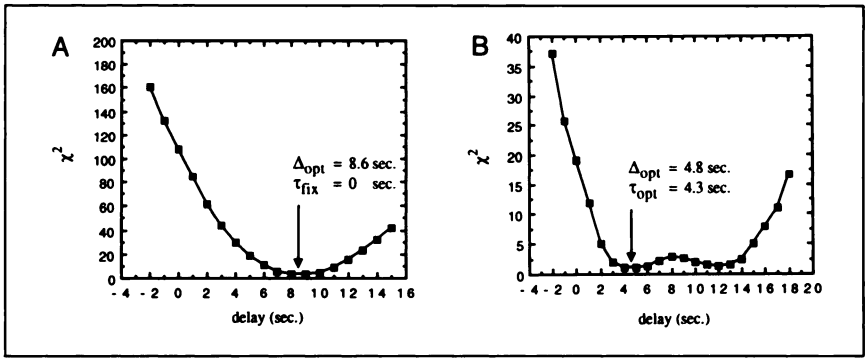

FIGURE 5. (A) Goodness-of-fit (χ^2) as a function of the assumed input function delay Δ if dispersion τ is neglected in the fit to the model function (Equation 8). (B) Goodness-of-fit (χ^2) as a function of the assumed input function delay Δ if dispersion τ is taken into account in the fit to the model function (Equation 8).

measurements. Figures 10A and 10B show the frequency distributions of flow and partition coefficient which result from fits to a total of 10^4 noisy data sets. The statistical uncertainties of the mean values are about 0.1%. The deviation of the mean flow from the true flow amounts to 0.4%, the corresponding deviation of the mean partition coefficient amounts to 2.2%.

For the generation of the partition coefficient distribution a sliding median filtering over the results of five consecutive fits in the simulation run was performed to remove outliers that occur due to known instabilities of the division p = f/k at this noise level.

Tissue Heterogeneity and Scan-Length Dependence

To quantitate the possible effects of tissue heterogeneity, we performed simulations by superimposing pure grey matter (f = 0.5 (ml/min)/ml, p = 0.9 ml/ml) and white matter (f = 0.2 (ml/min)/ml, p = 0.9 ml/ml) tissue-response curves. These were generated from a typical experimental input function for a scan length of 3 min according to our scan protocol (analogous simulations in the context of SPECT were recently performed by Yokoi et al. (*19*)). We obtained negligible underestimates (below 0.6%) of the mean flow for all admixtures of white matter between 0% and 100%. The maximum deviation of the partition coefficient from the true mean was a 14% underestimate at a grey matter fraction of about 30%.

The stated errors depend on the scan length; increasing the scan time to 5 min increases the maximum underestimate of the mean flow to 1.5%, whereas the maximum error of the partition coefficient decreases to 10%. These maximum deviations occur at a grey matter fraction of about 30%.

As is evident from the derivation of Equation 8 and Figures 2B and 3B, a variation in scan length does not result in systematic shifts of the parameter estimates in homogeneous tissue. However, scan length influences the precision of the estimates. This is illustrated by patient data in Figures 11A and 11B, which show dependence of the derived flow and partition coefficient on scan length for grey and white matter. The grey matter data are averaged values from the parietal cortex. Figure 11A shows that flow is determined accurately for scan lengths longer than 60 sec for both grey and white matter. A determination of the partition coefficient in white matter requires scan lengths of more than 150 sec, as shown in Figure 11B.

DISCUSSION

The Monte Carlo simulations were performed to evaluate bias of parameter estimates as a consequence of noisy-tissue data. Figure 10A illustrates that bias in the estimate of flow is negligible even for noise levels typical of the low count rates in individual pixels. Therefore the multilinear approach is equally suited for the processing of low noise ROI data as well as the generation of parametric images. The frequency distribution for the partition coefficient (Fig. 10B) shows a slight deviation from the Gaussian shape and a small shift (2.2%) of the mean with respect to the true value. Since the statistical accuracy in real studies is usually below this level, these systematic shifts can generally be ignored.

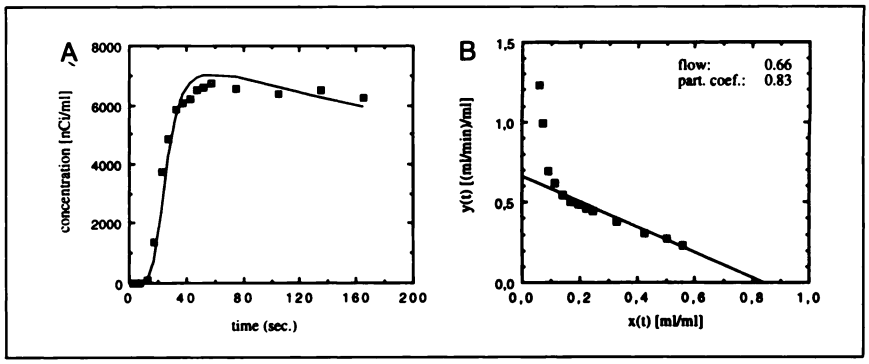

FIGURE 6. (A) Tissue response from Figure 1 together with fit according to Equation 8. Input function delay Δ and dispersion τ are fixed to values of 5 sec and zero, respectively. (B) Linearized representation of the data from (A) according to Equations 9 and 11. Large systematic deviations from the straight line occur as compared to Figure 2B because of erroneous correction of the input function delay Δ.

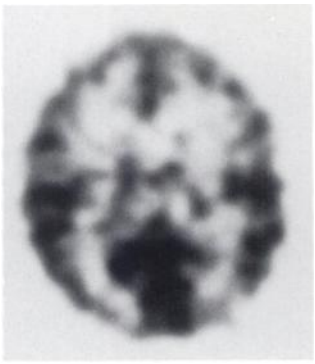

FIGURE 7. Transversal section of the brain in a patient with stenosis of the left middle cerebral artery postoperatively. Parametric blood flow image generated with the multilinear approach.

This finding has been independently confirmed for experimental data sets by comparing the parameters of fits to ROI data (the ROIs placed in regions of nearly homogeneous tracer kinetics) with averages obtained over the same ROIs in the corresponding parametric images. The results obtained agree very well.

Tissue heterogeneity due to limited spatial resolution plays a minor role in PET as compared to SPECT. The quantitation of possible effects showed that heterogeneity can lead to deviations from the true mean values as far as the partition coefficient is concerned. Flow values always deviate slightly from the true mean. The underestimate of the mean flow increases slowly with increasing scan time, whereas the underestimate of the mean partition coefficient decreases. This is explained by the fact that long scan times yield a more accurate determination of the effective partition coefficient which converges toward the true mean for sufficiently long scan times. This leads to the stated behavior.

Scan length variation influences precision of the parameter estimates but does not lead to systematic shifts in the multilinear approach. Our results show that flow values are accurately determined for scan lengths of more than 60 sec even in white matter. A reliable determination of the partition coefficient necessitates scan length of more than 150 sec.

This is a direct consequence of the fact that a sufficient approximation to equilibrium between tissue and blood is necessary to derive any information concerning the partition coefficient. The much slower response in white matter explains the experimental finding. As a consequence we recently have changed our protocol by extending the total scan duration to 5 min, which enables improved determinations of the partition coefficient in low-flow areas.

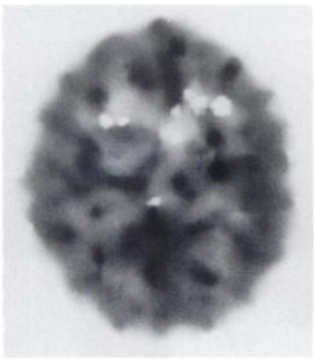

FIGURE 8. Parametric partition coefficient image corresponding to the blood flow image in Figure 7.

TABLE 1
Average Values (± s.d.) for Blood Flow and Partition Coefficient in Five Patients with Stenosis of the Middle Cerebral Artery

	Grey matter (parietal cortex)	White matter
Flow ((ml/min)/ml)	0.38 ± 0.09	0.21 ± 0.08
Partition coefficient (ml/ml)	0.75 ± 0.08	0.75 ± 0.08

The properties of the multilinear approach can be summarized as follows. A total of some 10–20 linear three-parameter fits (using a stepwidth of 1 sec for the delay Δ) determines all parameters of the model. The iteration count has the same order of magnitude as in nonlinear procedures, but the computational burdens per iteration step is reduced by a very large factor. In contrast to nonlinear minimization, our procedure determines the absolute minimum of χ^2 unambiguously and does not depend on good start values for all parameters to find this minimum. This is especially advantageous if one considers noisy data in which problems concerning the numerical stability of nonlinear procedures are encountered.

It should be stressed that this statement holds true even for the determination of the delay. In our approach this is the only parameter to be determined iteratively, therefore one can afford a grid search over the whole range of reasonable values. This becomes rapidly prohibitive if one extends the search to more than one parameter. Fitting N parameters in this way on a grid that is subdivided in a number of M intervals for each parameter does take a factor M^{N-1} longer than a one-dimensional search. Nonlinear algorithms must be used, understanding the stated problems in efficiency and stability.

Once delay is determined in a representative region, the same algorithm (linear three-parameter fit) can be used to determine dispersion, flow and partition coefficient on a pixel-by-pixel basis. This represents a unified procedure for ROI fits and calculation of parametric images. Although

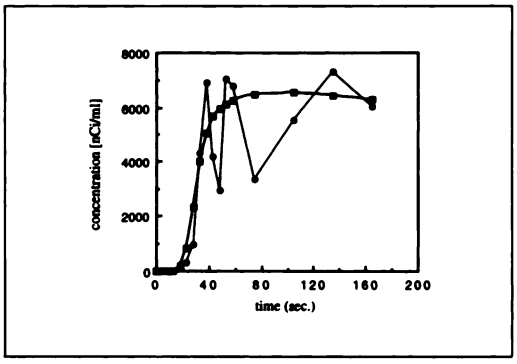

FIGURE 9. Simulated tissue response curves generated from a typical experimental input function using a flow of 0.5 (ml/min)/ml and a partition coefficient of 0.9 ml/ml. Shown are the ideal noise-free response (squares) and an example of a noisy response (circles). The standard deviation of the superimposed Gaussian-shaped noise is 20% at the maximum of the noise-free response curve.

FIGURE 10. (A) Frequency distribution of flow values. The distribution results from a total of 10^4 fits to noisy tissue response curves with a noise level of 20% (Fig. 9). The distribution is Gaussian-shaped. The mean shows no significant bias with respect to the true value. Accuracy of the mean is about 0.1%. (B) Frequency distribution of partition coefficient values. The distribution results from the same simulation as (A). For the partition coefficient a sliding median filtering over five consecutive results in the simulation run was performed in order to remove outliers. The distribution is slightly asymmetric and deviates from a Gaussian shape. The mean exhibits a bias of 2.2% with respect to the true value. Accuracy of the mean is about 0.1%.

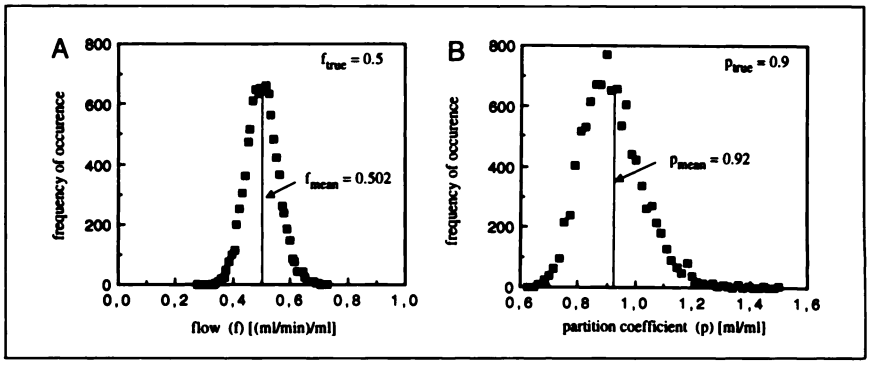

the fitting of ε as a third parameter on a pixel-by-pixel basis deteriorates the noise level of the images for f and k (or p), respectively to a certain extent, one gains the possibility of investigating the influence of regional variations of the dispersion constant τ on the results obtained for f and k.

In the vicinity of every fixed pair of values for delay and dispersion a small change of the delay Δ (for example, 1 sec) can effectively be compensated by a change in the dispersion constant τ to the opposite direction, with respect to the combined influence of Δ and τ on the fitted values for blood flow and partition coefficient. This reflects the fact that for not-too-large values of τ (below about 8 sec), the dispersion according to Equations 5 and 6 results in a shift of the input function, accompanied by only a relatively small distortion in shape. Consequently, allowing for a regional variation of ε (holding Δ fixed to the value derived from a fit to a representative region) effectively corrects for the regional variations of true dispersion and delay as long as stated restrictions concerning the range of Δ and τ are at least approximately fulfilled. As can be seen from the formal structure of Equation 8, the fitting of the parameter ε accounts also for a possible (arterial) fractional blood volume in the tissue space under investigation. Near larger vessels in which spillover effects play a role, the fitting of ε prevents serious bias in flow estimates.

The described procedure has been in routine use at our institute for about 1 yr. During this time more than 160 investigations with ^{15}O-labeled water have been performed. The procedure has proven to be well suited for clinical use because of its stability and speed. The ease of quality control by means of the linearized representation is especially useful and is an integral part of our implementation of the procedure. However it is not in general advantageous to use Equation 9 directly in the fitting procedure since it tends to introduce bias in the parameter estimates if delay values derived from ROI data do not fit exactly to each image pixel. The early deviations shown in Figure 6B lead to erroneous parameter estimates.

CONCLUSION

The multilinear approach described offers the opportunity to consistently correct effects of delay and dispersion in local blood flow measurements with dynamic PET. It is faster than nonlinear procedures and allows rapid generation of parametric images of blood flow, partition coefficient and the dispersion-time constant, once the delay is fixed by the same algorithm on a representative ROI. In comparison to weighted integration techniques for the generation of such images, the dynamic information of the PET scan seems to be used more efficiently in this approach. A suitable graphic display of the data enables a direct and sensitive evaluation of the consistency of data and model. These evaluations are highly desirable with respect to use of quantitative approaches in a clinical environment.

FIGURE 11. (A) Scan length dependence of flow determination. Averages of five patients are shown. Grey matter data are from the parietal cortex. Accurate determination of flow in grey and white matter is achieved for scan lengths longer than 60 sec. (B) Scan length dependence of partition coefficient determination. The same patient data as in (A) are used. Accurate determination of partition coefficient in grey matter is achieved for scan lengths longer than 90 sec. In white matter scan lengths of more than 150 sec are required.

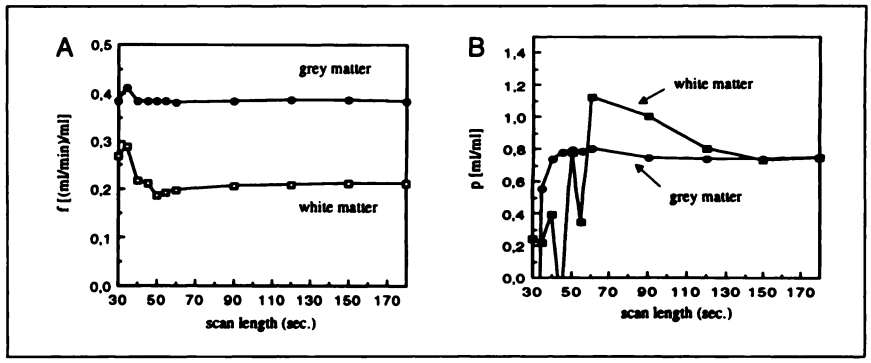

REFERENCES

1. Kanno I, Iida H, Miura S, Murakami M, Takahashi K, Sasaki H. A system for cerebral blood flow measurement using an $H_2{}^{15}O$ autoradiographic method and positron emission tomography. *J Cereb Blood Flow Metab* 1987;7:143–153.
2. Meyer E, Tyler JL, Thompson CJ, Redies C, Diksic M, Hakim AM. Estimation of cerebral oxygen utilization rate by single-bolus $^{15}O_2$ inhalation and dynamic positron emission tomography. *J Cereb Blood Flow Metab* 1987;7:403–414.
3. Meyer E. Simultaneous correction for tracer arrival delay and dispersion in CBF measurements by the $H_2{}^{15}O$ autoradiographic method and dynamic PET. *J Nucl Med* 1989;30:1069–1078.
4. Iida H, Higano S, Tomura N, et al. Evaluation of regional differences of tracer appearance time in cerebral tissues using ^{15}O-water and dynamic positron emission tomgraphy. *J Cereb Blood Flow Metab* 1988;8:285–288.
5. Lammertsma AA, Frackowiak RSJ, Hoffman JM, et al. The $C^{15}O_2$ build-up technique to measure regional cerebral blood flow and volume of distribution of water. *J Cereb Blood Flow Metab* 1989;9:461–470.
6. Iida H, Kanno I, Miura S, Murakami M, Takahashi K, Uemura K. Error analysis of a quantitative cerebral blood flow measurement using $H_2{}^{15}O$ autoradiography and positron emission tomography, with respect to the dispersion of the input function. *J Cereb Blood Flow Metab* 1986;6:536–545.
7. Press WH, Flannery BP, Teukolsky SA, Vetterling WT. Modeling of data. In: *Numerical recipes in C*. Cambridge: Cambridge University Press, 1988: 540–547.
8. Blomqvist G. On the construction of functional maps in positron emission tomography. *J Cereb Blood Flow Metab* 1984;4:629–632.
9. Yokoi T, Kanno I, Iida H, Miura S, Uemura K. A new approach of weighted integration technique based on accumulated images using dynamic PET and $H_2{}^{15}O$. *J Cereb Blood Flow Metab* 1991;11:492–501.
10. van den Hoff J, Burchert W, Müller-Schauenburg W, Hundeshagen H. Dynamische ^{15}O-H_2O PET zur bestimmung des LCBF: ein neuer ansatz zur generierung parametrischer bilder [Abstract]. *Nucl Med* 1992;31:A80.
11. Kety SS, Schmidt CE. The nitrous oxide method for the quantitative determination of cerebral blood flow in man: theory, procedure and normal values. *J Clin Invest* 1948;27:476–483.
12. Yokoi T, Iida H, Itoh H, Kanno I. A new strategy based on graphic plot analysis for rCBF and partition coefficient with iodine-123 IMP and dynamic SPECT validation study using O-15 and PET [Abstract]. *J Nucl Med* 1992; 33:911.
13. Dhawan V, Conti J, Mernyk M, Jarden JO, Rottenberg DA. Accuracy of PET rCBF measurements: effect of time shift between blood and brain radioactivity curves. *Phys Med Biol* 1986;31:507–514.
14. Herscovitch P, Markham J, Raichle ME. Brain blood flow measured with intravenous O-15 H_2O. 1. Theory and error analysis. *J Nucl Med* 1983;24: 782–789.
15. Koeppe RA, Hutchins GD, Rothley JM, Hichwa RD. Examination of assumptions for local cerebral blood flow studies in PET. *J Nucl Med* 1987; 28:1695–1703.
16. Raichle ME, Martin WR, Herscovitch P, Mintun MA, Markham J. Brain blood flow measured with intravenous $H_2{}^{15}O$. II. Implementation and validation. *J Nucl Med* 1983;24:790–798.
17. Huang SC, Carson RE, Hoffman EJ, et al. Quantitative measurement of local cerebral blood flow in humans by positron computed tomography and ^{15}O-water. *J Cereb Blood Flow Metab* 1983;3:141–153.
18. Matzke KH, Meyer GJ, Hundeshagen H. An advanced system for the administration of 15-O water. *J Labelled Compal Radiopharm* 1993;32:459–460.
19. Yokoi T, Iida H, Itoh H, Kanno I. A new graphic plot analysis for cerebral blood flow and partition coefficient with iodine-123-iodoamphetamine and dynamic SPECT validation studies using oxygen-15-water and PET. *J Nucl Med* 1993;34:498–505.